Material Analysis of Lead Free Solder Deposited by Electrochemical Deposition

Tom Ritzdorf, Sam Lee, Ian Drucker
Semitool Business Unit, Applied Materials
655 West Reserve Dr., Kalispell, MT 59901
(406) 758-7502 tom_ritzdorf@amat.com

Downloaded from http://meridian.allenpress.com/ism/article-pdf/2012/1/000136/2344056/isom-2012-ta45.pdf by guest on 23 November 2022

Abstract

Lead-free solders have essentially replaced lead-tin solders for new microelectronic applications. At the same time, many products are continuing to go through miniaturization, so the behavior of the solder material is changing as a function of the connection size. As lead-tin solder has been replaced by lead-free alloys, electrodeposited SnAg has become the standard solder alloy used on wafers. Tin-based solders exhibit a complex material structure in the deposit, as recrystallization occurs in the deposit, and as intermetallic compounds form. Understanding the complex nature of these materials is becoming increasingly important to the performance of our electronic products. We have characterized ECD SnAg solder alloy deposits in terms of composition, grain size, phase, microstructure, and texture using EBSD analysis. We will discuss the effects of modifying the process parameters on the microstructure which could implications on the performance of the solder bump as a chip-level interconnect. We have seen that the metals deposit as β-tin with finely dispersed intermetallic grains. We have also seen evidence of recrystallization of the deposit subsequent to deposition, although the recrystallization behaviour is significantly different than the well-characterized copper recrystallization. Finally, the metal at the interface below the solder reacts with Sn to form intermetallic compounds, the compositions of which are dependent on the materials present. The effects of the process parameters on the deposit properties are becoming increasingly important to understand in order to control the properties of the interconnection, and how it changes over its lifetime. We have characterized the incorporation of trace organic materials in the deposit as a function of plating parameters. The deposition of SnAg from an MSA-based plating bath is very different from the deposition of copper from a copper sulfate plating bath. We have noticed that the incorporation of organic additive materials, as well as the grain size, increases as the deposition rate is increased in the deposition of SnAg.

Keywords: Lead free solder, Materials analysis, ECD, Intermetallic compounds

Introduction

Over the last several years lead-free solders have essentially replaced lead-tin solders for new microelectronic applications. This has been driven by RoHS requirements to eliminate lead. As lead-tin solder has been replaced by lead-free alloys, electrodeposited SnAg has become the standard solder alloy used for flip chip, or C4, applications on wafers. Tin-based solders exhibit a complex material structure in the deposit, as recrystallization occurs in the deposit, and as intermetallic compounds form.

At the same time, many products are continuing to go through miniaturization and microbumps and micropillars are being introduced, especially in the drive to integrate through silicon vias to achieve 3D integration. This means that the behavior of the solder material is changing as a function of the connection size. It has been shown that the

volume of intermetallic compounds, as a fraction of a solder connection, increases as the solder volume decreases, which leads to changes in the thermo-mechanical properties of the solder joints. [1,2] Understanding the complex nature of these materials is becoming increasingly important to the performance and reliability of the electronic products that are becoming increasingly prevalent in our everyday lives.

This work involves the deposition of tin silver alloy on silicon wafers using equipment, chemistry and processes that are consistent with industrial processes used today to create flip chip bumps for chip interconnections. Bumps of various sizes have been plated and the composition and grain structure has been analyzed by several analytical techniques.

Experimental

Silicon wafers were used as substrates for plating processes, utilizing industry-standard ECD of SnAg solder structures. All wafers had oxide on the silicon surface, then were deposited with a Ti/Cu barrier/seed stack as part of the under bump metallurgy (UBM). The areas to be electroplated were then defined with a photolithography process that created a template for the ECD process. Depending on the feature sizes, a dry film photoresist or a spin-on photoresist was selected. Prior to ECD, all samples received a plasma descum process using an Axic Plasmastar RIE tool. All electroplating was accomplished using Applied Materials' Semitool Raider or Raider-S ECD tools. After plating, the photoresist was stripped. Analysis was either completed after the ECD and photoresist strip process, or the sample was subjected to a wet etch to remove the barrier/seed layers, and was reflowed in a Sikama reflow oven using flux for post-reflow analysis.

ECD processes were used to create the bumps and UBM structures on the samples analyzed. Any metal layers with thickness over one micrometer were deposited by ECD, and sequential depositions without drying the wafer were used to deposit Ni/SnAg, Cu/SnAg or Cu/Ni/SnAg structures. Copper ECD was performed using a sulfuric-acid based bath containing proprietary organic additives; nickel was deposited using a commercial nickel sulfamate bath; and the tin-silver solder alloy was deposited with a commercially available methane sulfonic acid based plating bath. ECD processes with a variety of average deposition rates for SnAg alloy deposition were used in order to characterize the impacts of deposition rate on various parameters of the solder structures. A cross-sectional micrograph of a Ni/SnAg solder bump can be seen in Figure 1. The light spots in the SnAg are intermetallic compound grains that are dispersed within the β-tin matrix. Most of these occur at the grain boundaries of the columnar β-tin grains.

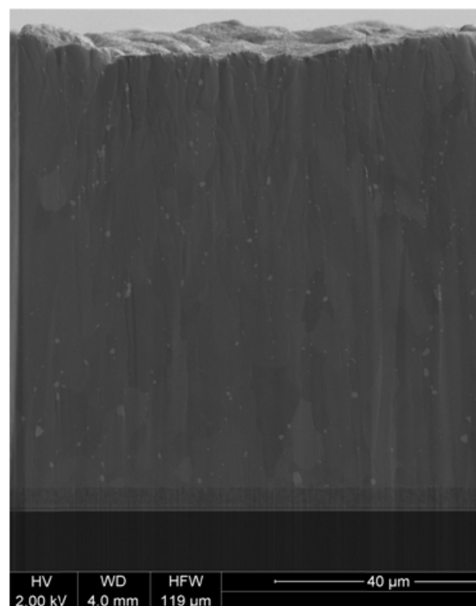

Figure 1. Cross-sectional SEM micrograph of a SnAg solder bump with a plated Ni UBM layer.

The samples were prepared using an FEI Helios600i SEM/FIB. The FIB(Focused Ion Beam) uses a Gallium liquid metal source. The FIB uses a 30kv beam at a maximum current of 65 nA. To prepare each sample an initial cross-section is performed to remove the bulk of the material which is followed by several cleaning cuts to smooth the surface. The total time to prepare each sample is approximately 2-3 hours. Immediately following the FIB cross-sectioning the samples were analyzed in order to minimize any contamination on the cleaned section. The FEI Helios600i utilizes two detectors for analysis, an EDS detector and an EBSD camera.

Downloaded from http://meridian.allenpress.com/ism/article-pdf/2012/1/000136/2344056/isom-2012-ta45.pdf by guest on 23 November 2022

The EDAX APOLLO X Silicon Drift Detector is an EDS (energy-dispersive X-ray spectroscopy) system which performs elemental analysis. This was used to differentiate between the materials when compiling the data so that a more accurate EBSD phase map can be created.

The EDAX Hikari EBSD (electron backscatter diffraction) system was utilized to acquire crystal orientation and phase, and to calculate the grain boundary locations and grain sizes. The energies used for analysis were generated by the SEM electron beam and ranged from 20-25kv at 1.4-5.5 nA. Each scan took from minutes to several hours, depending on the total area scanned and the step sized used. The step size was based on the average grain size and desired resolution in the scanned area.

The TOF-SIMS data presented here were collected using an IONTOF TOF.SIMS 5-300 instrument in dynamic mode using Cs sputtering and detection of negative secondary electrons. The sputtered area was 100x100 µm, which was a little larger than the solder bumps being analyzed, and the detection area was 25x25 µm. We analyzed the depth profiles and estimated the counts associated with a depth far enough below the surface as to avoid any surface contamination. The data was normalized to the counts of SnO_2^- in order to make the data semi-quantitative.

Results and Discussion

It is well-known that SnAg alloy deposition rate (or current density) plays a primary role in determining the composition of the plated alloy. Low concentrations of the more noble silver ions in the plating bath cause the silver to be deposited above the limiting current density of silver. Therefore, the amount of silver in the deposit is completely mass-transfer controlled. On the other hand, the tin is in much higher concentration, and is deposited under kinetic control. This means that as the deposition rate of the alloy in increased, the silver content in the deposit should decrease according to a 1/x behavior. This can be seen in Figure 2, which shows the average composition through the height of as-plated solder bumps by EDS analysis.

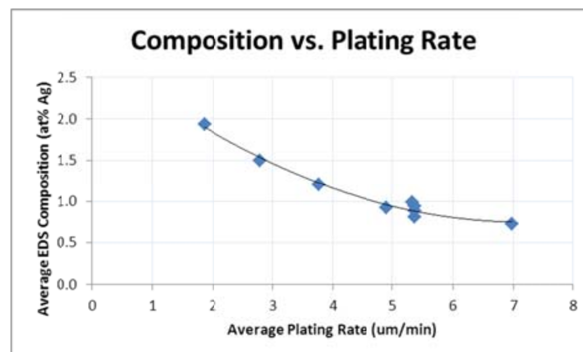

Figure 2. Average composition of solder bumps plated at varying average deposition rates, by EDS. The atomic percentage of silver was measured in multiple horizontal areas of a cross-sectioned solder bump and the values were averaged to create this curve.

Dynamic TOF-SIMS analysis was used to measure the amount of incorporated contaminants within the solder bumps after plating. We analyzed the average level of several contaminants at fixed distances below the surface in order to avoid surface contamination effects. Figures 3-5 and Table 1 show the impact of deposition rate of SnAg on the levels of contamination by organic materials, chlorine, and fluorine in the SnAg. This behavior appears to be different than the case of ECD copper in damascene interconnect applications in that the contamination level increases with increasing deposition rate, while in damascene copper ECD processes the contamination levels are generally seen to decrease as deposition rates are increased.

Table 1. SIMS analysis results.

Ion Detected	Deposition Rate (µm/min)		
	5.5	7.9	10.3
C_2H^-	15	30	50
CN^-	15	100	20
O^-	5000	1300	15000
F^-	30	90	600
S^-	6	25	22
Cl^-	7	15	18

Downloaded from http://meridian.allenpress.com/ism/article-pdf/2012/1/000136/2344056/isom-2012-ta45.pdf by guest on 23 November 2022

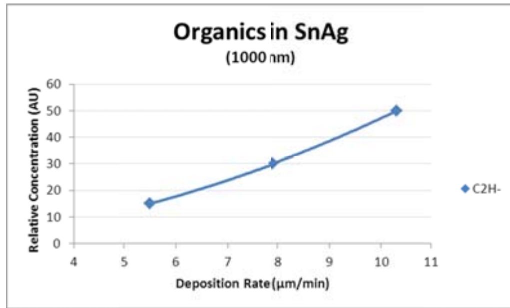

Figure 3.

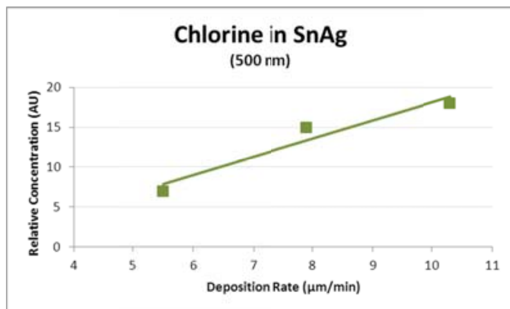

Figure 4.

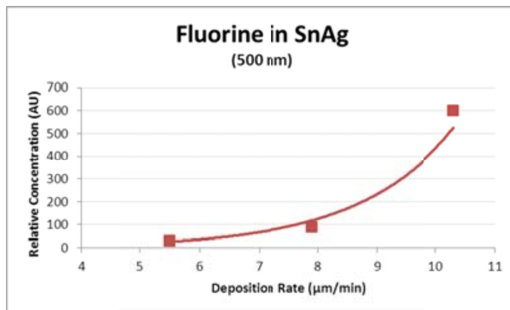

Figure 5.

The average grain size of the solder bumps was determined during the cross-sectional EBSD analysis of the bumps. In general, the solder structures are deposited in such a way as to create large, columnar grains that have high aspect ratios. The standard grain size calculations do not take these aspect ratios into account, but the analysis shows that the average grain size increases with increases in average current density of the solder deposition. This is seen in Figure 6.

Figure 7 shows the image quality map from the EBSD system. This map looks like an SEM micrograph, but it is actually a map of the relative fit of the EBSD signal to the material index files used. The lighter colored pixels represent a better fit of the acquired data to the material files. This image provides a good representation of the grain structure of the sample due to the fact that the fit parameters degrade at grain boundaries due to the diffraction data representing portions of two adjacent grains. The different materials are indicated in this figure, but that information is not obvious from the image itself. The image quality data is important in the cleanup phase of EBSD data analysis because it is used to remove misidentified pixels with low image quality, and to identify grain boundaries.

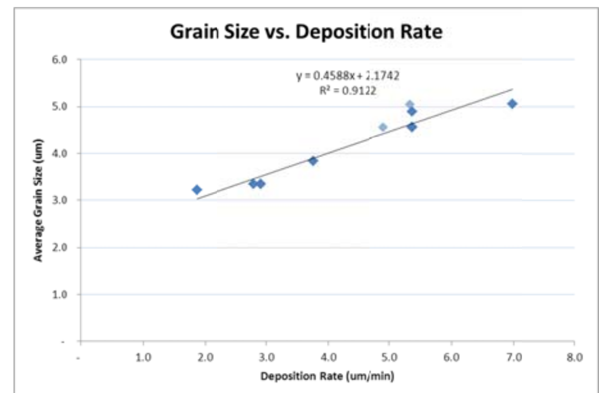

Figure 6. Average grain size of SnAg grains as a function of average solder deposition rate.

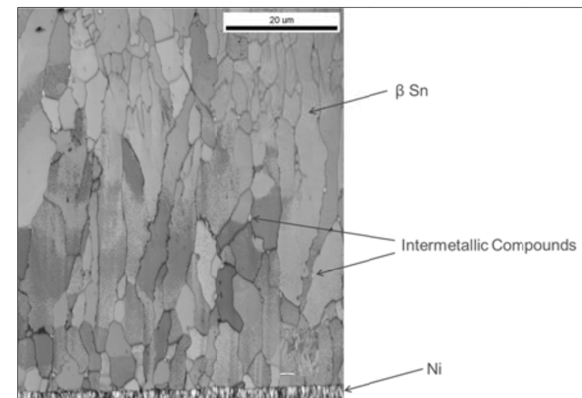

Figure 7. Image quality map of SnAg bump cross-section from EBSD analysis.

The EBSD Kikuchi patterns and corresponding Hough peak data are used to determine the phase and orientation of the individual grains scanned by EBSD. Figure 8 is a colored phase map which indicates the material phases identified by matching the

Downloaded from http://meridian.allenpress.com/ism/article-pdf/2012/1/000136/2344056/isom-2012-ta45.pdf by guest on 23 November 2022

diffraction data to the material index files chosen for the analysis. This phase information is shown along with locations of the grain boundaries determined by EBSD. The EDS data that was acquired simultaneously with the EBSD data was used to discriminate between very similar phases such as fcc copper and fcc nickel, whose lattice parameters and resultant diffraction patterns are almost identical. The EDS data is also used to map out regions of the sample with similar composition profiles and that information is used to limit the choice of material index files that are used to identify the phases of points in that region.

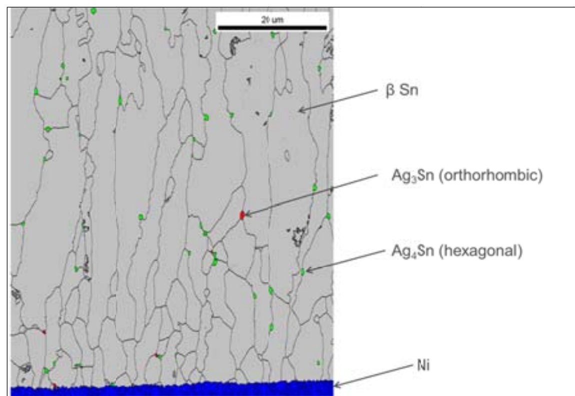

Figure 8. Phase analysis map of SnAg bump, showing β-tin, Ni, and AgSn intermetallic phases.

In Figure 8 it is obvious that the majority of the solder bump is made up of β-tin, with a thin (~3 μm) nickel layer underneath. There are also small grains of silver-rich intermetallic compounds dispersed within the matrix of the β-tin, mainly at the grain boundaries. These intermetallic compounds are typically identified as Ag_3Sn in most of the literature. [4,5] Interestingly, our EBSD analysis identifies most of these IMC crystals as the hexagonal Ag_4Sn compound, rather than the orthorhombic Ag_3Sn compound in this as-plated solder bump.

Regardless of the particular IMC phase present, the fact that the majority of the silver in the solder bump is already tied up to form the Ag_3Sn or Ag_4Sn IMC in the as-plated condition means that this silver is not available in the melt, until the temperature is increased beyond 480°C or 724°C, respectively, as seen in the phase diagram (Figure 9). Since these temperatures exceed the normal reflow temperature range by a large amount, the reflow process will melt the β-tin phase, which could contain up to 0.08 wt % Ag [3], but the IMCs will remain as solid particles suspended in the liquid solder ball. This means that the reflow of electroplated SnAg solder alloys will essentially be driven by the melting temperature of the β-tin phase, and will be relatively independent of the silver content in the alloy. It also means that the solder bump after reflow will be a composite material with particles of IMC that were in the initial electroplated deposit distributed within the crystal structure that results from the reflow process. Therefore, the majority of the IMC particles in a bump after reflow should be Ag_4Sn rather than Ag_3Sn.

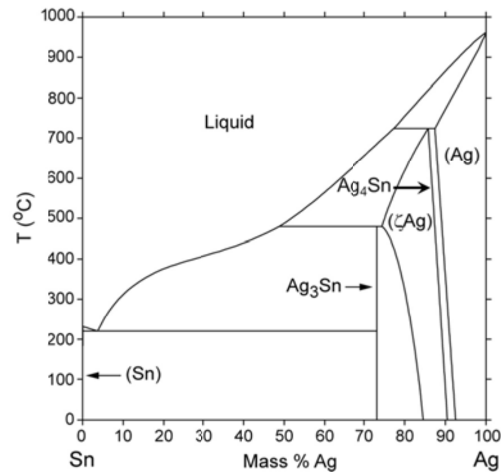

Figure 9. Tin-silver phase diagram (NIST).

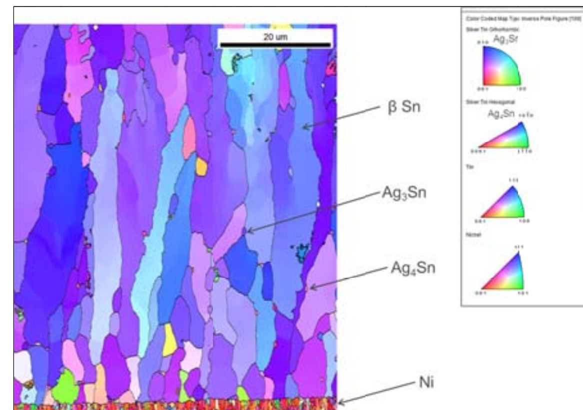

Figure 10. EBSD Inverse Pole Figure plot of Ni/SnAg solder bump with respect to the plane of the silicon wafer. The blue coloring indicates that the β-tin is strongly <110> oriented.

The usual use of EBSD data is to provide crystallographic orientation information. Figure 10 shows an inverse pole figure plot

Downloaded from http://meridian.allenpress.com/ism/article-pdf/2012/1/000136/2344056/isom-2012-ta45.pdf by guest on 23 November 2022

which indicates the crystallographic orientation of the materials on the silicon wafer. In order to have a useful set of data, it is important to look at the orientation with respect to the wafer plane, not the cross-section plane. When we do this, the inverse pole figure plot of Figure 10 shows clearly that there is a strong <110> orientation, or texture, of the β-tin grains. It can also be seen that the grains are smaller near the nickel interface (at the beginning of the solder deposition) and that they get larger and more anisotropic as the deposition preceeds. The β-tin grains at the beginning of the solder deposition also appear to be more randomly oriented. This is possibly due to the influence of the nickel, with the preferred orientation of the SnAg deposition taking over as the solder thickness increases.

If we want to focus more on the UBM layers, we can use a higher resolution EBSD scan, as seen in Figure 11. This image shows the bottom of the plated solder bump, with the ECD nickel layer on top of the PVD copper layer, as indicated on the right side of the image. Again, this is an inverse pole figure map of the cross-section with respect to the plane of the wafer. It is interesting to see that the PVD copper layer has a very strong <111> orientation, but the electrodeposited nickel on top of it has a <001> preferred orientation. This is rather surprising, considering that nickel and copper have almost identical lattice parameters (Copper has a lattice parameter of 3.61Å and nickel has a lattice parameter of 3.52Å.) and both have an fcc crystal structure. This is an indication that the nickel sulfamate ECD process has a stronger influence than the substrate that the nickel is being deposited on, in determining the preferred orientation of the nickel layer. The nickel also shows a columnar grain structure, with little evidence of twinning and recrystallization having taken place.

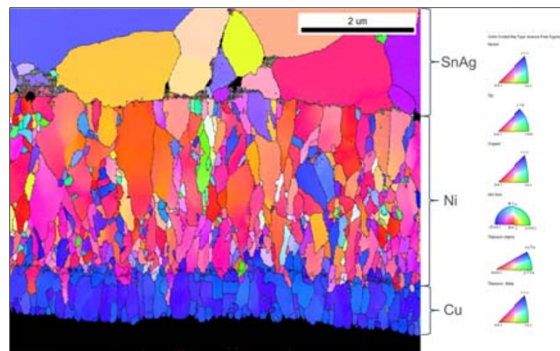

Figure 11. EBSD Inverse Pole Figure plot of the UBM area of the same solder bump in Figure 6, with respect to the plane of the silicon wafer. This image shows the orientation of the PVD Cu and ECD Ni layers beneath the SnAg bump.

Figures 12 and 13 show inverse pole figure maps similar to the one in Figure 10, with the focus on the SnAg material. These bumps were plated with successively higher current densities, which leads to higher plating rates. Again, we see that the columnar β-tin grains exhibit a stong <110> texture. The obvious difference between these images and Figure 10, though, is that there are a few very large grains of β-tin near the nickel interface. This is in contrast to the fact that we saw smaller β-tin grains near the nickel interface in Figure 10. We believe that these large tin grains are the result of recrystallization of the original small grains near the nickel interface. It has been well-characterized in ECD copper that recrystallization is driven largely by an excess of grain boundary energy associated with small, equiaxed grains. [6] It is expected that increased grain boundary energy associated with smaller grains of the electroplated SnAg would have a similar impact on driving grain recrystallization.

Downloaded from http://meridian.allenpress.com/ism/article-pdf/2012/1/000136/2344056/isom-2012-ta45.pdf by guest on 23 November 2022

Figure 12. EBSD Inverse Pole Figure plot of a Ni/SnAg solder bump showing large tin grains near the nickel surface.

Figure 13. EBSD Inverse Pole Figure plot of a Ni/SnAg solder bump showing large tin grains near the nickel surface.

Conclusions

Our analysis shows that each of the metal layers deposited exhibits a preferred orientation, and that this orientation may be determined more by the deposition process than by epitaxy with underlying layers. We have seen that SnAg deposited from an MSA-based chemistry deposits large, <110> oriented columnar β-tin grains with small grains of AgSn intermetallic componuds dispersed mainly at the grain boundaries. The size of the β-tin grains has been shown to be proportional to deposition rate. Hexagonal Ag_4Sn constitutes the largest portion of these IMCs. We have seen evidence of recrystallization of the β-tin grains near the interface with nickel.

We have determined that the metal composition of SnAg is empirically as expected from a bath that is mass transfer limited in silver, but exhibits kinetically controlled tin deposition. We have also seen that several of the incorporated contaminant species tend to deposit in greater concentrations as the current density, or plating rate, is increased.

Acknowledgements

The authors would like to thank Charles Wang for assisting with the EBSD analysis and several instructive discussions.

References

[1] J.P. Lucas, H. Rhee, F. Guo, and K.N. Subramanian, “Mechanical Properties of Intermetallic Compounds Associated with Pb-Free Joints Using Nanoindentation”, Journal of Electronic Materials, Vol. 32, No. 12, pp. 1375-1383, 2003.

[2] S.K. Kang, P. Laura, D. Shih, D.W. Henderson, J. Bartelo, T. Gosselin, S.R. Cain, C. Goldsmith, K. Puttlitz, T.K. Hwang, and W.K. Choi, “The Microstructure, Thermal Fatigue, and Failure Analysis of Near-Ternary Eutectic Sn-Ag-Cu Solder Joints”, Materials Transactions, Vol. 45, No. 3, pp. 695-702, 2004.

[3] H. Baker, ed., “ASM Handbook, Volume 3 Alloy Phase Diagrams”, ASM International, p. 2-37, 1992.

[4] J. Shen, Y. Liu, Y. Han, P. Zhang and H. Gao, “Formation of Bulk Intermetallic Compound Ag_3Sn in Slowly-Cooled Lead-Free Sn-4.0 wt pct Ag Solders”, Journal of Materials, Vol.21, No. 6, pp. 827-830, 2005.

[5] R.S. Sidhu and N. Chawla, “Three-dimensional microstructure characterization of Ag_3Sn intermetallics in Sn-rich solder by serial sectioning”, Materials Characterization, 52, pp. 225-230, 2004.

[6] T. Ritzdorf, L. Chen, D. Fulton, C. Dundas, Comparative Investigation of Plating Conditions on Self-Annealing of Electrochemically Deposited Copper Films, IITC 1999.

Downloaded from http://meridian.allenpress.com/ism/article-pdf/2012/1/000136/2344056/isom-2012-ta45.pdf by guest on 23 November 2022